5. 3-D NUMERICAL ANALYSIS OF FREQUENCY-DOMAIN AND TIME-DOMAIN CONTROLLED SOURCE ELECTROMAGNETIC METHODS IN MARINE ENVIRONMENT

5.1 INTRODUCTION

The 3-D seismic reflection method is a principal tool to explore for marine hydrocarbon reservoirs. It yields relatively high resolution information about the sub-bed structure and can identify structures that may contain hydrocarbon. However, the associated drawback of using seismic reflection method solely lies in not defining whether the potential hydrocarbon reservoir contains hydrocarbon or seawater. Approximately, 90% of the seismic finds contains water, and not of hydrocarbon and gas (Thirud, 2002).

EM methods have the potential to reduce the risk of drilling dry wells because they can distinguish seawater saturated reservoirs (low electric resistivity) from hydrocarbon-saturated reservoir (high electric resistivity) (Wright et. al., 2002). In the past, the sub-seafloor electric resistivity was mainly obtained as supplementary information by wire line logging of wells (Eidesmo et. al., 2002). However, utilizing non-invasive marine EM methods offer clear cost-effective advantages over conventional logging methods.

This numerical modeling study evaluated the sensing ability of the three different marine EM methods to sense a thin hydrocarbon reservoir in deep marine environments. The MMT, the marine FDCSEM and marine TDCSEM methods were selected in this study

and their synthetic responses and the related physics were investigated using numerical modeling techniques.

5.2 NUMERICAL MODELING METHODS

To investigate how marine EM methods sense a thin resistive hydrocarbon reservoir and what the factors governing their responses are, synthetic EM responses for the hydrocarbon reservoirs and background models were calculated using the two layered-earth analytical codes ((i) formulated by Ki-Ha Lee and (ii) provided by K. –M. Strack), a modified version of 3-D frequency-domain finite difference modeling code (Newman and Alumbaugh, 1995) and the parallel version of 3-D time-domain finite difference modeling code (Commer and Newman, 2004).

For the marine FDCSEM modeling, eleven source frequencies, from 0.01 to 1 Hz were considered, and five different 3-D finite difference grids were employed to simulate the different source frequencies. The average dimensions of these grids were 84 * 84 * 111 cells, and the smallest cell size in z-direction was 12.5 m (at high frequencies) or 25 m (at low frequencies) to handle large contrast of electric resistivity at the air-seawater interface and at the boundaries of the hydrocarbon reservoir. The largest cell size in the finite difference grids is set so it does not exceed 20 times the smallest cell size. These 3-D forward finite difference models were computed on UW-Madison's Condor platform, a large collection of distributively owned serial computers.

For the MMT modeling, ten different 3-D finite difference grids were employed to simulate the different source frequencies from 1E-4 to 0.4 Hz. The average dimensions of these grids were 80 * 80 * 120 cells. Again, the smallest cell size in z-direction of 12.5 m or 25 m was used to handle large contrast of electric resistivity at the air-seawater interface and at the boundaries of the hydrocarbon reservoir. All these 3-D forward models were computed on PC workstation platforms.

Synthetic EM responses of the marine TDCSEM method were computed by the parallel version of the 3-D FDTD code (Commer and Newman, 2004). The finest cell size near the source was 50m. Beyond the vicinity of the source, the cell size increases by a growth factor of 1.25 and finally, x, y and z boundaries were at ± 20 km. These large model dimensions were used so that the effects caused by boundary conditions could be neglected.

5.3 NUMERICAL MODELING RESULTS

5.3.1 1-D HYDROCARBON RESERVOIR MODEL

The 1-D reservoir model (Figure 5.1a) consists of a 100 m thick, 100 Ohm-m layer representing a hydrocarbon reservoir, embedded at a depth of 1km below a 0.7 Ohm-m seafloor. A 1km thick, 0.3 Ohm-m seawater layer overlies the seafloor. As the background model (Figure 5.1b), the same seafloor model was employed without the reservoir.

The marine FDCSEM method employed a 250 m long, 100 A, x-directed HED which was placed 950 m below the air-water interface. Seafloor EM receivers were densely deployed on the seafloor in a grid pattern with 400 m spacing. The electric receiver noise level is set to $1.0E^{-10}$ (V/m) and the magnetic receiver noise level to $1.26E^{-5}$ (nT) (Ed Nichols, personal communication). The marine TDCSEM method utilizes the same survey configuration as the marine FDCSEM method employs. The same size time-domain HED is employed instead of the frequency-domain HED and the ramp-off time is set to $1.0E^{-4}$ seconds.

5.3.1.1 THE MARINE MAGNETOTELLURIC METHOD

For the MMT method, the apparent resistivity plots are calculated and compared for the background and 1-D reservoir models in Figure 5.2. The true resistivity contrast between the background sediment and the hydrocarbon reservoir varies from 5 to 200. Although the conversion of the synthetic data into apparent resistivities is a normalization procedure, the apparent resistivity can be a good approximation to actual subsurface resistivity and thus, apparent resistivity plots can serve to evaluate how the MMT method is sensitive to a thin hydrocarbon reservoir. If there is no significant difference in the apparent resistivity of the two models, the MMT method is deemed inappropriate for the detection of such a resistive hydrocarbon reservoir (Pellerin et. al., 1996).

Figure 5.2 shows that the MMT method is insensitive to the thin resistor and the response for the conductive sediment is dominant. Figure 5.2 also demonstrates the insensitivity of

the MMT method to the variation of the electric resistivity of the reservoir. There is little change in response as the resistivity contrast between the reservoir and its surrounding increases beyond a ratio of 10:1 (Hoversten et al, 1998).

In order to explain this characteristic of the MMT method, the electric field and current density vector along the 2-D cross-section are plotted at 0.04 Hz in Figures 5.3 and 5.4, respectively. In Figure 5.3, there is no noticeable difference in the electric field distribution between the background model and the 1-D reservoir model. This is because the source fields consist of purely horizontal fields as shown in Figure 5.3, and horizontal electric fields should be continuous along resistivity boundaries. Therefore, the current density distribution plots of the 1-D reservoir model (Figure 5.4b) merely show the thin missing layer of current density in the place of the 1-D reservoir, and the overall current distribution patterns, between the two models, are the same as Figure 5.4. As a result, the electric and magnetic responses on the seafloor are essentially the same for the two models. This modeling result indicates that the MMT technique can not solely sense the presence of the 1-D hydrocarbon reservoir as its response depends mainly on the inductive response.

5.3.1.2 THE MARINE FREQUENCY-DOMAIN CONTROLLED SOURCE ELECTROMAGNETIC METHOD

5.3.1.2.1 HORIZONTAL ELECTRIC FIELD RESPONSE

To understand how the marine FDCSEM method senses a thin resistive target, synthetic EM responses for the background and 1-D reservoir models were generated. Figure 5.5 shows the in-line and broadside x-directed electric field amplitudes (E_X) calculated at the seafloor for both the background and 1-D reservoir models. The normalized responses shown in Figure 5.5d are computed by dividing the 1-D reservoir responses by the background responses.

As source-receiver separations increase in Figures 5.5a and 5.5b, the Ex of the background model decays exponentially on a semi-log plot up to approximately 4.9 km in separation. Beyond this distance, the slope of E_X for the background model becomes constant on the same plot. Notice that this distance also corresponds to the position of the last inflection point on the E_X phase curves for the background model shown in Figure 5.5c. At larger separation values, the E_X phase for the background model becomes constant as the slopes of the E_{X_IP} and E_{X_OP} for the background model decay at the same constant rate.

When the E_X plot for the background model is compared to that of the 1-D reservoir model, it is possible to separate response into the three distinct zones. For separation

distances from 0 km to 1.4 km, there is no difference between the two model responses. From 1.4 km to 4.9 km, the 1-D reservoir model starts to produce larger responses than the background model, and the difference in the amplitudes between the models grows until the source-receiver separation distance reaches about 4.9 km. Beyond 4.9 km, the gap between the two curves starts to narrow. As a result, the peak of the normalized E_X field occurs at 4.9 km (Figure 5.5d) when the reservoir responses are normalized by the background responses. The difference in the position of the peak between in-line and broadside configurations is insignificant, but there is a large difference in the peak amplitudes between both configurations.

To help explain the observation in Figure 5.5, cross-sectional views of the electric field in both models are shown in Figure 5.6 (the in-line configuration) and Figure 5.7 (the broadside configuration).

First, the xz cross-sectional view of the in-line electric fields at y=0 (m) is examined in Figure 5.6 to explain the response of the inline configuration. In the vicinity of the HED (zone 1), the induced electric field of the background model is identical to that of the 1-D reservoir model. The seafloor receivers close to the source in both models record the same E_X field which mainly passes through the seawater and partly through very shallow seafloor sediment. Hence, the E_X plots for both models overlap each other up to 1.4 km on the X-axis in Figures 5.5a and 5.5b. Beyond this point, the amplitude and direction of the seafloor electric field in the 1-D reservoir model is different from that of the background

model, as seafloor receivers start to sense the electric responses that are affected by deep seafloor sediment.

The HED-induced electric field drives both horizontal and vertical currents in the conductive marine media. As vertical current is normally incident upon the boundary of the horizontal reservoir, charge buildup occurs along the boundary in order to satisfy one of the electromagnetic boundary conditions: continuity of normal current. The electric fields from these charges: (i) superimpose on the initial HED induced fields, (ii) distort the geometry of the initial induced fields, and (iii) contribute extra strength of electric field to the seafloor receivers. Hence, the electric field measured on the seafloor for the 1-D reservoir model is much larger than that for the background model.

When the 3-D geometry of the electric fields of the HED is considered, it is obvious that the inductive responses dominate the broadside configuration. On the yz cross-section of the two models at x=0 (m) in Figure 5.7, the electric field produced by the HED is induced horizontally around the reservoir without being incident upon it. Comparing to Figure 5.6, there is less difference in the seafloor electric field distributions between the two models. Thus, the inductive dominated response of the broadside configuration yields a much smaller anomaly than that of the in-line configuration (Figure 5.5d). Note that strong anomalous E_X fields are developed along the upper and lower boundaries of the reservoir in Figures 5.7c and 5.7d but they do not affect the electric fields on the seafloor.

Next, where the normalized peak amplitude occurs in Figure 5.5d is directly related to the effect of the air-seawater interface. The diffusing EM wave from the source arrives at the air-seawater interface, then propagates in the air along the interface without attenuating as the resitivity in the air can be assumed to be infinity. Thus the only decrease in its amplitude in this path occurs due to geometrical spreading. However, as it propagates through the air it continually excites EM energy to be 'refracted' back into the seawater. The critical angle of refraction is nearly 90°, resulting in the lateral EM wave, or the so called airwave, in the seawater (Eidesmo et al., 2002). Note that this strong airwave contains no information about the seafloor resistivity structure.

The airwave dominates the seafloor EM response when the source-receiver offset is much larger than the sea-water depth. This is possible because the airwave propagates with minimal loss in energy though the air while the seafloor EM response is significantly attenuated in the conductive media. Thus at those distances where the airwave is the dominant arrival at the seafloor, the decay rate of the measured EM fields appears to be smaller on a semi-log plot (Figure 5.5). As a result, the gap between the E_X values for both models begins to decrease at around 4.9 km and thus the peak of the normalized electric field occurs at this same distance. In addition, the phase of the electric field becomes constant as the phase of the airwave does not change as it propagates across the air-seawater interface. Thus, the peak location is also where the phase of the background seafloor response becomes constant. For convenience, FDCSEM critical distance is

defined as the point where the maximum value occurs and (or) the point where the phase of the background field becomes constant.

A few factors control where the FDCSEM critical distance exists. The primary factor to determine the FDCSEM critical distance is the depth of seawater. The airwave is attenuated more rapidly in a thicker water column before it reaches the seafloor. As a result, the seafloor EM response can withstand masking effect of the airwave even at larger source-receiver offset. Hence, the FDCSEM critical distance becomes more distant from the source in deeper marine environment. Lower source frequencies and a more resistive background of the seafloor also make the FDCSEM critical distance larger because of low attenuation of the seafloor EM responses in conductive media.

To illustrate how the peak location changes with different model parameters, the locations of the maximum normalized electric fields are calculated as a function of source frequency, sea depth and background resistivity of the seafloor in Figure 5.8. The peak location is determined uniquely by the background model parameters. However, the peak amplitude is a function of the size of the resistive reservoir, its depth, and source strength, and can not be tabulated as a universal reference.

Next, a number of source frequencies ranging from 0.01 Hz to 10 Hz were employed to calculate the normalized E_X responses shown in Figure 5.10 for the same models. As the source frequency increases, the normalized responses become very narrow for the largest

amplitude peaks. At very low and very high frequencies, the marine FDCSEM method does not yield favorable results. To evaluate what happens at the extremes of frequencies investigated, the 2-D electric field responses were calculated and plotted in the same way as done in Figure 5.6 for the lowest and highest frequencies (0.01 Hz in Figure 5.11 and 10 Hz in Figure 5.12).

At 0.01 Hz, the vertical currents develop broadly and the FDCSEM response comes from a much larger volume of the subsurface and seawater. Thus, the FDCSEM responses tend to lack resolution for the structures of interest. At 10 Hz in Figure 5.12, the vertical electric fields that are above the receiver noise level are very localized in the vicinity of the source due to attenuation. Elsewhere, the effects of attenuation make the electric field too small to consider. In addition, the horizontal electric fields due to the airwave exists even at large depths below the seafloor in Figures 5.12a and 5.12b. As a result, at the higher frequencies, there is no noticeable effect of the 1-D reservoir on the seafloor electric field seen in Figures 5.10, 5.12c and 5.12d. Hence the 10 Hz source fails to sense the target.

In the described 1-D modeling study, the frequencies from 0.4 Hz through 1 Hz yield the best survey results. Although other higher frequencies, between 1 and 10 Hz, show larger responses (Figure 5.10), using these frequencies in practice is limited by the receiver noise level. This will be discussed later.

Electric field distributions at 0.63 Hz are shown in Figure 5.6. The vertical currents develop high concentration around a depth of 2 km, the target depth in Figures 5.6a and 5.6b. Thus, the vertical currents can efficiently interact with the horizontal layer. As a result, the 0.63 Hz source yields a noticeable and measurable difference of the electric field amplitude on the seafloor between the two models.

Another interesting feature shown in Figure 5.10 is the sharp, high magnitude peaks of the normalized response at the frequencies of 2.5 Hz and 4.0 Hz. To investigate this feature, the E_X response for the in-line configuration along the survey line, and the cross-section of the electric field distribution at 2.5 Hz were plotted in Figure 5.13. It is clear that in Figure 5.13a, the dip of the E_X plot around 4 km from the source for the background model causes this sharp peak. Comparing Figure 5.13a to Figures 5.13b and 5.14c, it is seen that dips of E_{X_IP} plot and E_{X_OP} plot correspond to the location of a phase reversal in both the $E_{X\ IP}$ and the $E_{X\ OP}$ on the seafloor. If E_{X_IP} and E_{X_OP} change their phases at approximately the same location on the survey line, the E_X plot for the background model has the dip, resulting in an additional peak. For convenience, this additional peak is defined here as 'phase reversal peak.' In Figure 5.13a, the location of the phase reversal is close to the FDCSEM critical distance. Thus, this phase reversal peak superimposes on the peak due to the FDCSEM critical distance, yielding the sharp peak in Figure 5.10a. From this, it is possible to predict what happens if a phase reversal peak is far from a FDCSEM critical distance. In this case, the peak of the normalized E_X may not occur only at the

FDCSEM critical distance but where the phase reversal of the field occurs. Furthermore, the phase reversal peak can be larger than the peak due to the FDCSEM critical distance.

To this point, the normalized E_X response along a single survey line has been analyzed to understand the physics of the marine FDCSEM method. Due to the 3-D nature of the HED-induced fields, it is worth analyzing the normalized horizontal electric field responses over the entire seafloor. The amplitude of the total horizontal electric field, $\sqrt{Ex^2+Ey^2}$ was calculated on the seafloor in both models and then normalized at a few selected frequencies (Figure 5.14). Note that at 2.5 Hz, the peak of the normalized response can not be measured in practice with current technology due to receiver noise level. Again the two facts that were verified along a single survey line are double-checked: the sensing ability of the marine FDCSEM method in broadside configuration is poor compared to that of the in-line FDCSEM configuration. In addition, the peak location of the normalized horizontal electric field is mainly defined by the boundary beyond which the phase of E_X for the background model becomes constant due to airwave.

5.3.1.2.2 VERTICAL ELECTRIC FIELD RESPONSE

A conventional marine EM receiver is designed to measure horizontal EM fields on the seafloor. However, the behavior of the vertical component of the electric field on the seafloor is of interest in this study. Considering the geometry of an x-oriented HED-induced field, the vertical component of electric field does not exist along the broadside (y-oriented) survey line or is too small to be measured in a practical sense. Hence, only

the E_Z response for the in-line configuration is shown in Figure 5.15. This result illustrates that the vertical electric field measurement can be a useful additional measurement for the marine FDCSEM survey. Notice that there is no effect of the airwave on the vertical electric fields because the airwave is totally horizontal. A number of source frequencies ranging from 0.01 Hz to 10 Hz are employed to calculate the normalized E_Z responses for the same models in Figure 5.16 and Figure 5.17. Huge normalized E_Z responses along the in-line survey line are observed, as E_Z of the background model, the denominator of normalization process, reduces to zero beyond its FDCSEM critical distance.

5.3.1.2.3 HORIZONTAL MAGNETIC FIELD RESPONSE

Magnetic field responses are an additional and useful measurement for CSEM methods. The difference of the magnetic fields between the background and reservoir models depends on how the HED-induced currents in conductive seawater and below conductive seafloor are distorted by the 1-D reservoir as the different current flow patterns produce different magnetic fields at a given point.

Figure 5.18 shows the B_Y field response of the two models along the in-line and broadside survey line on the seafloor. As with the electric fields, the normalized magnetic field response for the in-line configuration behaves differently from that for the broadside configuration.

First, the response for the in-line configuration is observed in Figure 5.18a. For a source-receiver separation from 0 km to 1.6 km, there is no difference in B_Y amplitudes between the two models. From 1.6 km to 6.1 km, the 1-D reservoir model starts to give larger response than the background model. The difference in the B_Y amplitudes between the models gets larger until the source-receiver separation distance reaches 6.1 km. As the slope of the B_Y component for the background model becomes less steep at 6.1 km, the gap between the two plots starts to narrow. As a result, the peak of the normalized B_Y field occurs at 6.1 km (Figure 5.18d). The B_Y phase of the background model also becomes constant around 6.1 km in Figure 5.18c. Compared to the normalized E_X field for the in-line configuration (Figure 5.5d), it is distinctive that the normalized B_Y field for the in-line configuration (Figure 5.18d) has the second peak around 4.2 km on the source-receiver separation axis.

To explain the observation in Figure 5.18, cross-sectional views of the complex B_Y field are presented in Figure 5.19 for the two models. The 1-D reservoir model produces fields that are laterally stronger than that of the background seafloor model, resulting in large normalized B_Y response on the seafloor. Because this anomalous magnetic response is the direct result from the difference in the current patterns between the two models, it is required to analyze induced current distribution, as shown in Figure 5.20 which is very similar to induced electric fields in Figure 5.6. As the vertical currents interact with the horizontal resistive reservoir, charge buildup occurs along the upper and lower boundaries of the reservoir. This extra charge buildup on the surface of the reservoir produces an

increase in electric potential which can drive currents in conductive media. Therefore, more intense current flows are developed above and below the 1-D reservoir in Figures 5.20c and 5.20d. As a result, the 1-D reservoir model yields larger a magnetic field than the background model.

The two interesting differences between the normalized magnetic fields (Figure 5.18) and the normalized electric fields (Figure 5.5) are that (a) the width of the normalized magnetic fields is broader than that of the normalized electric fields, and (b) the normalized magnetic field has the dual peaks.

The reason for the broad width of the anomaly in the normalized magnetic fields is due to the fact that, in the near and intermediate zones of the source, the decay rate of the magnetic field is smaller than that of the electric field. For example, in the near field zone which is the domain of small values of R, the amplitude of the magnetic field decreases approximately as $1/R^2$ while the amplitude of the electric field decreases as $1/R^3$ (where R is the radial distance from the center of the dipole to the measurement point). As a result, the magnetic field curve has broader width than the electric field. This broad pattern of the magnetic field may be considered unfavorable from the detection point of view of a sharp anomaly due to the reservoir. However, this slower decay rate has an advantage: the magnetic field has better opportunities to overcome ambient electromagnetic noise and receiver noise problem. For example, the electric field for the in-line configuration for the 1-D reservoir model can be measured up to 8.5 km from the source location in Figure 5.5

while the magnetic field for the in-line configuration for the 1-D reservoir model can be measured over 10 km from the source location in Figure 5.18.

In order to determine what causes the secondary peak of the normalized magnetic field for the in-line configuration in Figure 5.18d, it is necessary to observe the background B_{Y_IP} and B_{Y_OP} plots in Figure 5.18a. It is obvious that the phase reversal of B_{Y_IP} and B_{Y_OP} is responsible for gentle decrease in the slope of B_Y (the black-dashed contour) in Figure 5.18a. For the normalized electric field response in Figure 5.10a, the phase reversal of the seafloor E_{X_IP} and E_{X_OP} occurs around the FDCSEM critical distance, and hence, we see a single peak. However, if the phase reversal occurs away from the FDCSEM critical distance, dual peaks can be produced. As for the broadside configuration in Figure 5.18d, the peaks of the normalized B_Y field occur at around 3.6 km due to sign reversal and at around 5.6 km due to the FDCSEM critical distance on the source-receiver separation.

The broadside magnetic fields in the background and the 1-D reservoir models in Figure 5.21 show less difference at the seafloor-seawater interface than those in Figure 5.19. Hence the normalized peak for the broadside configuration is relatively small in Figure 5.18d. This is because the nearly horizontal currents around the seafloor on the x=0 cross-section for the broadside configuration are not distorted as much by the 1-D reservoir as for the in-line configuration. Notice that strong anomalous J_X fields are developed along the upper and lower boundaries of the reservoir in Figures 5.22c and 5.22d but the perturbation tends not to reach the seafloor.

To illustrate how the peak location changes with different model parameters, the locations of the maximum normalized magnetic field were calculated as a function of source frequency, sea depth and background resistivity of the seafloor in Figure 5.23. The overall pattern of the plots in Figure 5.23 follows what is expected: the peak location gets close to the source location as the source frequency increases, water depth decreases, and resistivity of seafloor decreases.

The corresponding peak amplitudes for cross-referencing are presented in Figure 5.24. For completeness in the 1-D modeling study, a number of source frequencies ranging from 0.01 Hz to 10 Hz were employed to calculate the normalized B_Y responses in Figure 5.25. When the 2-D normalized horizontal magnetic field plots with noise level contour of magnetic receiver are observed at a few selected frequencies (Figure 5.26), the frequencies from 0.4 Hz through 1 Hz are chosen as the optimal frequency band for the magnetic field analysis. Note that the noise level contours of the magnetic receiver in Figure 5.26 cover a larger area than that of the electric receiver in Figure 5.14 because the decay rate of the magnetic field is smaller than that of the electric field within the shown source-receiver separation (non-perfect far field zone). In Figure 5.26, the peak locations correspond well to boundaries beyond which the B_Y phase becomes constant.

5.3.1.3 THE MARINE TIME-DOMAIN CONTROLLED SOURCE ELECTROMAGNETIC METHOD

In order to compare the marine TDCSEM method to the marine FDCSEM method, the time-domain HED source, and any other modeling parameters were kept identical to those used in the marine FDCSEM modeling. The only difference is that the step-off synthetic responses for the background, the 1-D reservoir, and the 3-D reservoir models were computed.

The in-line E_X and E_Z responses are shown in Figure 5.27, the broadside E_X and dB_Y/dt responses in Figure 5.28, and the in-line dB_Y/dt and broadside dB_Z/dt responses in Figure 5.29. The marine TDCSEM method senses the presence of the 1-D reservoir. However, the observed difference in the in-line E_X responses between the 1-D reservoir and background models in Figure 5.27a-c are relatively small, and most of the differences are a DC response in early time rather than a transient response within the decay. The broadside E_X measurements in Figure 5.28 are also overwhelmed by a DC response, and show more complicated responses with a sign-reversal. This is because the E_X receivers in the broadside configuration initially record the return currents, which has the opposite direction to the source polarization in early time, but then are affected by the image current at late time.

While the horizontal magnetic field measurements at the air-land interface can not sense a thin resistor at depth as discussed in Chapter 4, the horizontal magnetic field

measurements (Figure 5.28d-f and 5.29a-c) on the seafloor sense the presence of the 1-D resistive reservoir. This is possible because the transient vertical currents are not canceled out at the seawater-sediment interface, and hence both horizontal and vertical transient currents contribute to the measured horizontal magnetic fields on the seafloor. In contrast, the vertical magnetic field measurements (Figure 5.29d-f) along the broadside survey line do not discern the 1-D reservoir because they are generated by horizontal current flows.

Compared to the marine FDCSEM in-line E_X responses (Figure 5.5), the marine TDCSEM in-line E_X responses suggests a poorer sensing ability than the marine FDCSEM method even though time-domain responses should be transformable into frequency domain ones using Fourier's theorem (Cheesman et al., 1987). These counterintuitive results can be explained by the fact that the step-off transient response consists of the Fourier Transform of 1/(f*FD(f)) where f is the frequency, and FD(f) represents the frequency-domain response. Thus the high frequency signals which are most sensitive to the reservoir are down-weighted.

This small difference of the measured responses between the two models in the marine TDCSEM method is verified by viewing the current distribution between the background model (Figure 5.30) and the 1-D reservoir model (Figure 5.31). In both models, the strong horizontal transient currents are mainly confined in the most conductive seawater, and this current distribution dominates the overall responses in the two models. The electric field snapshots are also shown in Figure 5.32 for the background model and in Figure 5.33 for

the 1-D reservoir model. Even though the charge build-up along the boundary due to vertical currents produces strong electric fields, colored as red, near the reservoir, the effect of these electric fields is limited around the reservoir boundary, and thus its contribution to the seafloor electric field is insignificant.

An alternative to the step-off is to analyze the impulse response which can be approximated by taking the time-derivative of the step-off response. The impulse response should provide better results due to the fact that higher frequency information is introduced through the impulsive source current. This argument is also applied to explain why the time-derivatives of the horizontal magnetic fields (Figure 5.29) senses the reservoir better than the in-line horizontal electric field responses (Figure 5.27).

The time-derivatives of the in-line E_X and E_Z responses are plotted in Figure 5.34, and the time-derivatives of the broadside E_X response in Figure 5.35. They indicate the presence of the 1-D reservoir more clearly than the step-off responses (Figure 5.27). The electric field response for the background model in Figure 5.34 consists of two parts (Edwards, 1988). The first perturbation is caused by the fast diffusion of the EM field through the less conductive marine sediment, and the second perturbation is by slow diffusion through the most conductive seawater. As the source-receiver separation becomes shorter, the electric field perturbation by the diffusion through the marine sediments is overlaid with the perturbation by the diffusion through the seawater. The two-path diffusion becomes more visible as the source-receiver separation becomes larger. This is because the

difference in diffusion velocity between the two media is highlighted at larger offset. However, it is suggested to find an optimal source-receiver separation rather than to choose the possible largest source-receiver separation, because the impulse signal becomes smaller and broader due to dispersion with distance.

This two-path diffusion of the impulse EM signal helps the TDCSEM method to overcome the 'air-wave' problem associated with the FDCSEM method in shallow marine environments. The 1-D FDCSEM and TDCSEM responses with varying seawater depth are shown in Figure 5.36. The FDCSEM method does not work effectively at shallow seawater depth because the airwave dominates the seafloor EM responses. As for the TDCSEM method, the two-path diffusion phenomenon becomes complicated in shallow water by the effects of the air but there are still large differences between the responses with and without the 1-D reservoir. This is possible because the seawater response lags behind the seafloor response due to the difference of electric conductivity between the seafloor and the seawater.

Shown in Figure 5.27 and 5.34, the vertical electric field (E_Z) measurement can be a useful additional measurement for the TDCSEM method. The smaller amplitude of E_Z implies that developing more sensitive seafloor receivers and more powerful transmitters is a critical factor to measure E_Z on the seafloor successfully. As for the time-derivatives of the broadside E_X responses in Figure 5.35, it is difficult to define the two-path diffusion visually in the same way as done for the time-derivative plots of the in-line E_X responses.

This is because the effect of sign reversal becomes dominant when time-derivative of the broadside E_X response is taken.

5.3.2 3-D HYDROCARBON RESERVOIR MODEL

For a more realistic marine EM forward model, the previous 1-D hydrocarbon reservoir is replaced by a 3-D anticline reservoir. The description of the 3-D hydrocarbon reservoir and the associated survey configuration are shown in Figure 5.37. All other modeling parameters for the 3-D forward modeling were kept the same as the 1-D forward modeling for consistency.

5.3.2.1 THE MARINE MAGNETOTELLURIC METHOD

The MMT apparent resistivity and impedance phase plots for the background and 3-D reservoir models are given in Figure 5.38. The Z_{XY} mode corresponds to the impedance calculated using x-directed electric field and y-directed magnetic field. In this study, the Z_{XY} response is the same as the Z_{YX} response when the Z_{XY} response is rotated by 90 degrees due to the two fold symmetry of the 3-D reservoir. Shown in Figure 5.38, the MMT method is not useful in detecting the anomalous responses due to the 3-D hydrocarbon reservoir.

Meanwhile, the sides of the 3-D reservoir are delineated better on the y=0 plane in the xy apparent resistivity plot than on the y=0 plane in the yx apparent resistivity plot. In order

to explain this characteristic of the MMT method, the Z_{XY} electric field and current distribution plots for the 3-D reservoir model are presented in Figure 5.39. Comparing Figure 5.38a to Figure 5.4, the telluric currents around the 3-D reservoir sides do contain a normally incident component upon the sides of the reservoir. When these currents interact with the sides, charge buildup occurs along the boundaries of the reservoir sides in order to satisfy one of the EM boundary conditions: continuity of normal current. The electric fields from these charges distort the local electric field slightly. However, the boundary charges do not contribute to the Z_{YX} response because the Z_{YX} electric field is parallel to the strike direction of the sides of the reservoir. As a result, the Z_{YX} response on the y=0 plane does not sense the boundary of the reservoir as well as the Z_{XY} response on the y=0 plane. This modeling study clearly demonstrates that boundary charges play an important role in the amplitude of a resistive reservoir anomaly.

Another interesting aspect of the MMT technique is the spatial variation of the vertical electric field on the sea floor when the section below the sea floor contains 2-D or 3-D inhomogeneity. Hoversten et al (1998) theoretically explained that vertical electric field measurements on the sea floor may be a useful additional measurement for the MMT method in order to detect 2-D or 3-D structures, because, at the sea-floor interface, the vertical component of electric field can be non-zero. In this study, the ratio of vertical electric field to horizontal electric field was computed along the profile at 0.04 Hz in Figure 5.40. This ratio value will be zero if the section below the sea floor is 1-D. Figure 5.40 illustrates that the vertical electric field measurement is sensitive to the presence of 2-

D or 3-D inhomogeneity below the seafloor. However, this measurement may not be useful in practice because of its small amplitude. For example, at x=1.1 km, the amplitude of the vertical electric field is only 2% of that of the horizontal electric field.

5.3.2.2 THE MARINE FREQUENCY-DOMAIN CONTROLLED SOURCE ELECTROMAGNETIC METHOD

5.3.2.2.1 ELECTRIC AND MAGNETIC RESPONSES

Figure 5.41 shows the normalized horizontal E field response of the 3-D reservoir model at four different x-oriented HED positions along the survey line on the x-axis (colored green in Figure 5.37b): (0 m, 0 m, 950 m), (1000 m, 0 m, 950 m), (2000 m, 0 m, 950 m) and (3000 m, 0 m, 950 m). Comparing the normalized electric field responses here to those from the 1-D reservoir modeling in Figure 5.14, the 3-D reservoir modeling results yield a few interesting features. The peak amplitudes of the normalized electric fields of the 3-D reservoir model are much smaller than those of the 1-D reservoir models, and vary with source position. The normalized field responses of the 3-D reservoir model decrease relatively quickly after the peak, while the normalized field responses of the 1-D reservoir model fall off more gradually.

To understand the difference of the normalized responses between the 1-D and the 3-D reservoir models, 2-D electric field distribution plots (Figure 5.42) and the 2-D current distribution plots (Figure 5.43) were plotted for the background, 1-D and 3-D reservoir

models. Two different x-oriented HED positions, (0 m, 0 m, 950 m) and (2000 m, 0 m, 950 m) were employed for the 3-D reservoir model.

Figures 5.42 and 5.43 imply that the magnitudes of the normalized horizontal electric fields in Figure 5.14 and 5.42 are related to the location of the hydrocarbon reservoir with respect to the highest concentration of the HED-induced vertical currents. In the case of the 1-D reservoir in Figure 5.43b, all vertical components of the HED-induced currents at 1000 m depth below the seafloor interact with the infinite horizontal slab of the reservoir. Therefore, the degree of charge-buildup on the surface of the 1-D reservoir is maximized. The additional electric fields from these electric charges are vector-superimposed on the electric fields from the HED, resulting in the large normalized electric field response shown in Figure 5.14.

If the 1-D reservoir is replaced by the localized 3-D reservoir shown in Figure 5.37, the degree of charge buildup depends on whether the high concentration of vertical currents can reach and interact with the reservoir effectively or not. For example, in Figure 5.43c, the 3-D reservoir is placed where the horizontal component of HED-induced currents are dominant. As a result, the minimal charge buildup on the surface of the 3-D reservoir does not significantly affect the electric field patterns between Figure 5.42a and Figure 5.42c. Thus the amplitude of the normalized horizontal electric field is insignificant in Figure 5.41a.

In contrast, when the HED position is changed from (0m, 0m, 950m) to (2000m, 0m, 950m) in Figure 5.43d, a high concentration of the currents normal to the reservoir boundary effectively interacts with the reservoir in the left side of the HED. Thus, a more distorted and higher amplitude electric field pattern is observed in Figure 5.42d, resulting in a larger normalized response in Figure 5.41c. Because the marine FDCSEM response is very dependent on source-receiver configuration when sensing a small localized hydrocarbon reservoir, high source-position density is required to ensure good coupling to the reservoir.

In order to analyze the horizontal electric field responses for the 3-D reservoir model in more detail, the seafloor E_X, E_{X_IP}, E_{X_OP} and phase plots along the y=0 survey line for a source, (2000 m, 0 m, 950 m) are plotted in Figure 5.44. The FDCSEM critical distance for the background model defines the peak location of the normalized field at -2.8 km. In the 3-D reservoir model, the charge buildup around the finite 3-D reservoir just slightly extends the FDCSEM critical distance beyond that of the background model. Thus, beyond this critical distance, the amplitude of the electric field of the 3-D reservoir model quickly converges to the background value. As a result, the anomalous response after the peak is roughly confined between the two FDCSEM critical distances.

When the x-directed HED is towed along the diagonal survey line in Figure 5.37b, the normalized response looks more complicated as shown in Figure 5.45. Figures 5.41 and

5.45 illustrate that it is very difficult to predict the real boundary of the 3-D reservoir from the normalized response in practice.

Figure 5.46 shows the normalized horizontal magnetic field responses over the 3-D reservoir. The overall pattern of the normalized horizontal magnetic fields is very similar to that of the normalized horizontal electric fields. The major benefit of using horizontal magnetic field response is that the noise level contour of magnetic receiver in Figure 5.46 theoretically allows for greater aerial coverage compared to that of the electric receiver in Figure 5.41. For the completeness in the 3-D reservoir modeling, the electric and magnetic responses for the same 3-D reservoir model with the y-oriented HED are shown in Figures 5.47 and 5.48 respectively. Again, these plots demonstrate that the amplitude of the FDCSEM response is very dependent on source-receiver configuration and the maximized response occurs when the survey configuration provides max-coupling of the normal currents to the reservoir.

The vertical electric field responses for the 3-D reservoir model and normalized amplitudes are presented in Figure 5.49. As the source-receiver separation increases in Figures 5.49a and 5.49b, the vertical electric field responses for the 3-D reservoir model start to be distinguishable from those for the background model, indicating the presence of the 3-D reservoir. In addition, its receiver level contours cover roughly the same region as those for the horizontal electric fields in Figure 5.41a and 5.41c. Thus, vertical electric

field measurements on the sea floor will be a useful additional measurement for the marine FDCSEM method.

5.3.3.2.2 EFFECTS OF 2-D BATHYMETRY

Seafloor topography is an additional parameter that will affect the results of the marine FDCSEM method. Irregular topography does not allow seafloor EM receivers to be at the same depth from the air-seawater interface, and can also produce different electric field distributions locally in the seawater column. In this sub-section, the 1-D and 3-D reservoir models employed previously have a simple 2-D bathymetric profile introduced as shown in Figure 5.50. This 2-D bathymetric profile includes an exaggerated vertical cliff. As the background model, the same 2-D seafloor model was used without the reservoir. The other modeling parameters and the description of the reservoir are the same as those described in the previous sub-sections.

The horizontal E field responses of the 1-D reservoir model (Figure 5.50a) were computed at two x-oriented HED locations: (-2000 m, 0 m, 950 m) and (2000 m, 0 m, 950 m). When the HED is placed at (-2000m, 0m, 950m), the asymmetry of the normalized E_X responses (Figure 5.51c) clearly shows how this simple topographic change affects the marine FDCSEM results. The survey line on the right side yields larger normalized E field response since the seafloor EM receivers on the right side of the HED are closer to the 1-D reservoir than those on the left side. In contrast, the peak location from the source on the right side is not significantly different from that on the left side. Figure 5.51c suggests that the topographic effects mainly come from the receiver-reservoir distance and not

from the airwave effect. This argument can be verified directly by viewing the 2-D electric field plots in the background and 1-D reservoir models shown in Figure 5.52. The forward modeling results at the other HED position are shown in Figures 5.53. The same explanation can be applied to Figure 5.53c. Besides the analysis of the E field responses, the B field responses are shown in Figure 5.54 for completeness in the modeling study. As explained before, they are basically the same as the E field responses but their width is broader than E field responses.

For a more realistic investigation for the topographic effect, the previous 1-D reservoir was replaced by the 3-D reservoir (Figure 5.50b). The E and B field responses for the model were computed, and then compared to those for the 1-D flat seafloor model bearing the same 3-D reservoir. Figure 5.55 clearly shows that the peak magnitude is highly affected by seafloor topography as well as the size of the reservoir, and the coupling of vertical currents to reservoir. Thus, the magnitude of the seafloor response can not be interpreted accurately without bathymetry information.

Figure 5.55 illustrates how the topographic variation of the seafloor can affect the normalized response in the marine FDCSEM survey, and suggests that high quality topographic information should be collected for any marine FDCSEM survey.

5.3.2.3 THE MARINE TIME-DOMAIN CONTROLLED SOURCE ELECTROMAGNETIC METHOD

The time-derivatives of the horizontal magnetic fields (B_Y), the horizontal and vertical electric fields (E_X and E_Z) for the in-line configuration are computed for the 3-D reservoir model in Figures 5.56, 5.57 and 5.58 respectively. In order to examine the effect of the different geometrical coupling of the vertical transient currents to the 3-D hydrocarbon reservoir, the time-domain HED source was placed at the center of the reservoir, (0 km, 0 km, 0.95 km) and at the edge of the reservoir, (2 km, 0 km, 0.95 km). The source-receiver separations were 1 km, 4 km, and 8 km. The time-derivatives of the electric and magnetic responses for the broadside configuration were similar to those for the in-line configuration but yielded much smaller difference. Thus, they were not considered in this sub-section.

The computed responses in Figures 5.56, 5.57 and 5.58 are analogous to the marine FDCSEM responses for the 3-D reservoir model. That is, the anomalous responses due to the 3-D reservoir model are much smaller than those due to the 1-D reservoir, and vary with source positions relative to the body. Even though analytical and numerical forward modeling codes that can compute the impulse response are not currently available, making it impossible to generate the current distribution-snapshots for the impulse source, viewing the current distribution snapshots for the step-off source provides alternative insights to understanding Figures 5.56, 5.57 and 5.58.

The current distribution snapshots around the 3-D reservoir for the two source positions, (0 km, 0 km, 0.95 km) and (2 km, 0 km, 0.95 km) are presented in Figures 5.59 and 5.60 respectively. As the time-domain HED is moved from the center of the reservoir (Figure 5.59) to the edge of the reservoir (Figure 5.60), the vertical transient currents in the seafloor are coupled to the reservoir more efficiently, producing the larger anomalous responses as seen in Figures 5.56b, 5.57b and 5.58b.

Like the marine FDCSEM method, the marine TDCSEM method is very dependent on source-receiver configuration when over and adjacent to a small localized 3-D reservoir, and the diffusion angle of the vertical transient currents should be considered as an important survey factor to maximize the anomalous perturbation in the response.

5.4 CONCLUSIONS

Two types of galvanic source marine EM methods, the marine FDCSEM method and the marine TDCSEM method, have been investigated numerically, and compared to the MMT method.

As perceived in recent publications, the MMT method can not be used solely to determine if a seismic find is a hydrocarbon reservoir or brine reservoir. The primary reason for this failure is that the MMT method mainly relies on the inductive effect of horizontal source field which is inherently insensitive to thin resistors. The MMT method can at most

determine the vertical boundaries of a reservoir, if the structure of the reservoir changes rapidly in 3-D space, and thus the sides of the reservoir can cause charge buildup on themselves.

In contrast to the MMT method, the marine FDCSEM method is very sensitive to thin resistive hydrocarbon reservoirs at depth, since the response is both galvanic and inductive. The peak location of the normalized EM response is a function of source frequency, seawater depth and background resistivity of seafloor.

The peak magnitude of the normalized EM response depends on whether the high concentration of vertical currents can reach and interact with the reservoir effectively or not. Therefore, the normalized EM response of a localized 3-D reservoir is inherently much smaller than that of a 1-D reservoir. When the potential hydrocarbon reservoir has a strong 3-D nature and is localized, survey design becomes very important so that the vertical current can be more efficiently coupled to a localized 3-D reservoir yielding a maximized galvanic effect. Receiver noise level is also an important factor for successful survey design. The major benefit of using horizontal magnetic field response is that the noise level contour of the magnetic receiver theoretically allows for greater aerial coverage compared to that of the electric receiver.

The FDCSEM bathymetry modeling suggests that good quality bathymetry data should be collected during the survey cruise for an accurate interpretation of the FDCSEM data, because the magnitude of EM responses is noticeably affected by change of bathymetry.

The marine TDCSEM method is another promising EM geophysical tool for marine hydrocarbon exploration. Its response can be explained by two-path diffusion of the initial excitation through the more conductive seawater and the less conductive seafloor. When a 1-D resistive reservoir is inserted into the background model, the vertical transient currents interact with the horizontal resistive reservoir, producing charge buildup which causes the perturbation of the background electric fields. In order to enhance the degree of the anomalous perturbation, a proper transient EM pulse is required such that the relatively higher frequencies required for reservoir detection are produced. In this study, the time-derivatives of the step-off responses were taken alternatively to mimic the impulse source responses. Like the marine FDCSEM method, the marine TDCSEM method is also very sensitive to source-receiver configuration because the magnitude of the anomalous response depends on whether the vertical transient currents can be coupled to the reservoir efficiently or not.

This modeling study exemplifies that the vertical electric field measurements on the sea floor can be a useful additional measurement for both the marine FDCSEM and TDCSEM methods. In contrast, the vertical electric field measurement is not useful for the MMT method since its amplitude is too small to be measured in practice.

5.5 FIGURES

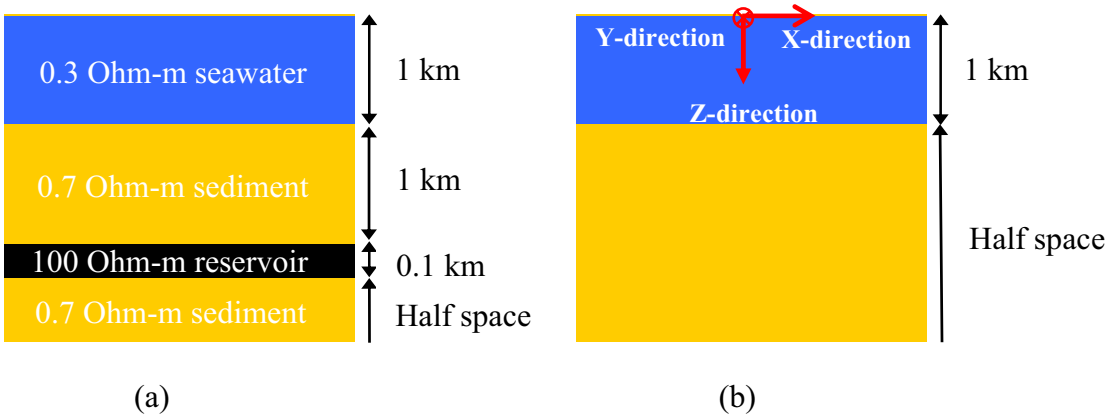

Figure 5.1. The 1-D seafloor models. (a) the 1-D reservoir model and (b) the background model.

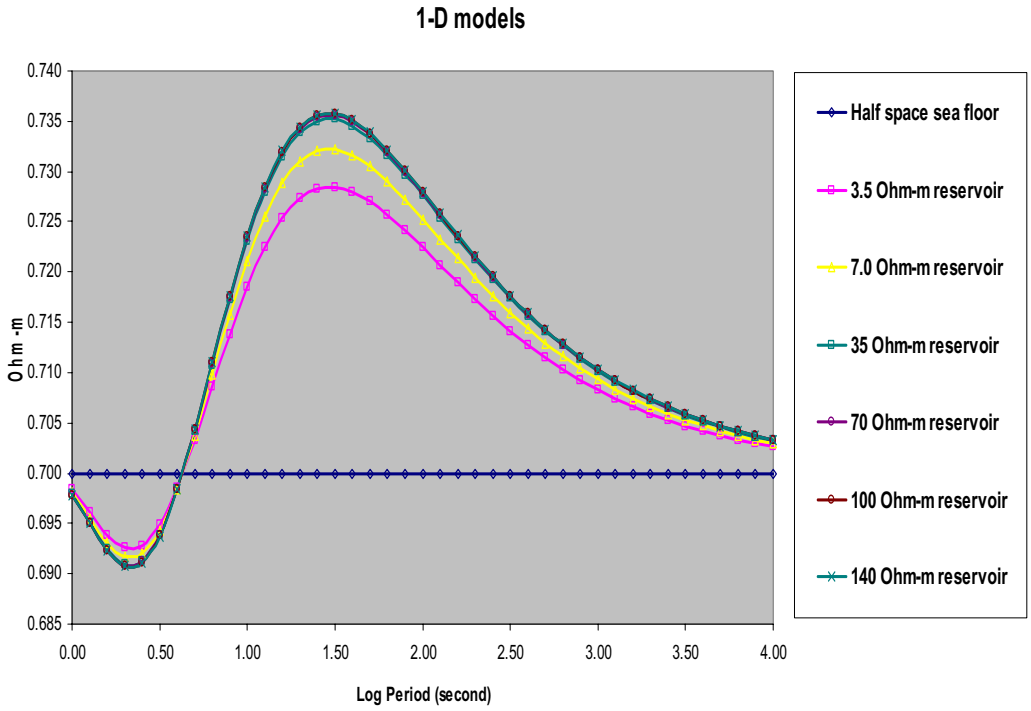

Figure 5.2. MMT apparent resistivity sounding curves for the background and 1-D reservoir models. The resistivity of the reservoir varies from 3.5 Ohm-m to 140 Ohm-m.